RESEARCH PAPER

Numerical and experimental characterization of a button-shaped miniaturized UHF antenna on magneto-dielectric substrate

MARTINO ALDRIGO[1], ALESSANDRA COSTANZO[1], DIEGO MASOTTI[1], CARLO BALDISSERRI[2], IOAN DUMITRU[3] AND CARMEN GALASSI[2]

The design and characterization of a new broadband small patch antenna, based on an innovative magneto-dielectric material and suitable for wearable applications at 868 MHz, is presented. To reduce antenna dimensions, while preserving its radiation and matching performance, a barium-strontium hexaferrite $Ba_{0.75}Sr_{0.25}Fe_{12}O_{19}$ has been synthesized as the antenna substrate to achieve magnetic permeability double than vacuum in the band of interest. First material realization is characterized and dispersive permittivity and permeability behaviors are included in the design of a small patch antenna with a shorting-plate. A button-size realization is obtained and its suitability for wearable applications is numerically and experimentally demonstrated on body with and without the presence of conductive shielding. Very good agreement with measurements is demonstrated for both matching and radiation performance of the antenna.

I. INTRODUCTION

In the last 10 years, a growing interest in wearable and implantable devices has been shown, since they can be exploited for applications in Body Area Networks (BANs): BANs are of great importance for real-time monitoring of health parameters, e.g. blood pressure, breathing rate, etc.

The challenge in the development of new integrated radio frequency (RF) systems is the miniaturization of all components: this is a mandatory requirement in order to build easy-to-wear or implantable devices. The drawback is that miniaturization affects the radiating performance and a trade-off between antenna reduced dimensions and performance needs to be reached, since electrically small antennas could not accomplish low-power link-budget requirements. A highly exploited solution to build miniaturized and non-invasive antennas is the patch antenna mounted on a dielectric substrate, thanks to its low-profile. Several solutions have been proposed for reduction of the patch size [1], but are not sufficient to fulfill wearable/implantable applications. A further miniaturization could be achieved by adopting ceramic substrates with high values of relative permittivity ε_r. The reduced effective wavelength λ_g is obtained at the

expense of an increased patch-ground plane coupling, thus reducing the field fringing effect: in this way, the radiating properties of the antenna may be degraded and the patch behaves more as a microstrip resonator. Indeed a significant reduction of radiation resistance is observed, which causes a decay in radiation efficiency. At the same time too low an antenna impedance is obtained, which is difficult to match.

By means of magneto-dielectric (MD) materials, antenna dimensions can be reduced as well, by exploiting relative magnetic permeability μ_r greater than unit, keeping ε_r at reasonable values. In this way the same miniaturization factor is obtained without affecting the above mentioned performance, since the refraction index n is defined as

$$n = \sqrt{\varepsilon_r \mu_r} \Rightarrow \lambda_g = \frac{\lambda_0}{\sqrt{\varepsilon_r \mu_r}}. \qquad (1)$$

In particular, the material characteristic impedance η_i can be kept in a range allowing easy antenna matching, since

$$\eta_i = \eta_0 \sqrt{\frac{\mu_r}{\varepsilon_r}}. \qquad (2)$$

Furthermore, radiating performance improvement, due to increased radiation resistance, and a wider bandwidth are observed.

MD materials can be classified into two main groups: meta-materials and composite materials. When using, for example, Embedded-Circuit Mediums as meta-materials [2, 3], one has to carefully take account of some crucial issues, such as

[1]D.E.I., University of Bologna, Viale Risorgimento 2, 40136 Bologna, Italy. Phone: +39 051 2093059
[2]CNR – ISTEC, Via Granarolo 64, 48018 Faenza (RA), Italy
[3]CARPATH, Faculty of Physics University "Al. Ioan Cuza", Carol I Boulevard 11, 700506 Iaşi, Romania
Corresponding author:
A. Costanzo
Email: alessandra.costanzo@unibo.it

properly embedding high-Q resonant loops in low-permittivity substrates and mutual couplings among embedded loops. Furthermore, mutual couplings between loops and antenna metallization inductance affect the permittivity of the dielectric substrate.

On the other hand, composite materials such as ferrites [4] have natural magnetic properties, which can be optimized during the synthesis process, thus allowing the desired trade-off between high values of μ_r and the ferro-magnetic resonance (FMR) at higher frequencies with respect to meta-materials. The most significant shortcoming of ferrites is represented by high magnetic losses at microwave frequencies, which have to be taken into account for the best performance prediction of devices designed on such composite substrates.

Hereinafter we always refer to the complex relative permittivity ε_r and permeability μ_r:

$$\varepsilon_r = \varepsilon' - j\varepsilon'' \text{ and } \mu_r = \mu' - j\mu''. \tag{3}$$

Our work describes the synthesis of an MD material (barium-strontium hexaferrite) to be used as the substrate for design of a small patch antenna with an overall size suitable for wearable applications [5, 6]. The material was prepared at CNR-ISTEC, Faenza, Italy and permittivity and permeability measurements of the material were carried out at the Faculty of Physics of University "Al. Ioan Cuza", Iaşi, Romania by standard instrumentation with reference samples. Then, the characterization has been repeated by means of resonance methods [7] while preparing the antenna layout and therefore using the actual antenna dimensions with the engineered MD substrate.

Our goal was to obtain a minimum value for the refractive index n of about 3.2, by means of the best trade-off between the ε_r and μ_r values. In Section II, material selection and manufacturing are discussed; the measured values of ε_r and μ_r are compared to the dispersive models implemented in the electromagnetic (EM) simulation tool; finally, an in-depth investigation on magnetic properties is presented. In Section III, antenna CAD design and prototype realization are described. In Section IV, a comparison between simulations and measurements of the antenna performance is discussed, together with experimental results on link-budget performance. In the Appendix, the measurement set-up is described in detail.

II. MD MATERIAL MANUFACTURING AND CHARACTERISTICS

A) Material selection and processing

Hexaferrites show a magnetoplumbite-similar crystal structure (i.e. cubic-hexagonal) [4], with high magneto-crystalline anisotropy and a preferred direction of magnetization. Different correlations between crystal and magnetic properties give rise to a further classification into S, M, W, Y, Z, and X types, which are characterized by: (1) a high coercive field, typical of "hard" permanent magnets; (2) magnetic losses damping the FMR, as a consequence of the anisotropy of single-crystals structure, where the shift of the resonance frequency depends on the orientation of the applied field w.r.t.

the principal crystal axes. The resonance band is broadened especially in polycrystalline materials, with randomly oriented crystals. In polycrystalline materials, further contributions to the band broadening derive from grain boundaries, porosity or in-homogeneities. The advantage in using hexaferrites consists in the high-frequency FMR due to their moderate values of relative permittivity and permeability, large anisotropy field, and low eddy-current losses. In particular, we concentrated on M-type hexaferrites whose strong anisotropy allows us to extend the frequency limit expressed by Snoek's law, i.e. a higher FMR can be observed as a large anisotropy (elliptically-polarized) field H_K is applied:

$$\omega_r^{min} \mu_i' = \gamma 4\pi M_S \sqrt{\frac{H_{K\vartheta}}{H_{K\phi}}}, \tag{4}$$

where μ_i' is the static permeability (i.e. the initial value of μ', which is assumed to be constant up to the FMR), ω_r^{min} is the minimum (angular) FMR, $\gamma = 1.76 \times 10^6$ rad/sec·Oe is the gyromagnetic constant, M_S is the saturation magnetization and $H_{K\vartheta}$, $H_{K\phi}$ are the cross-polar and co-polar components of H_K (respectively) w.r.t. the easy-plane of magnetization. It is of primary importance to utilize the MD substrate well below the FMR, in order to avoid strong energy absorption and quick variations in permeability values. In practical applications, such materials exhibit non-negligible magnetic losses in the microwave frequency band, and have a complex crystalline structure which has to be carefully controlled during the synthesis process.

As a first substrate to be tested for the band of interest, we have chosen the barium-strontium hexaferrite with the composition $Ba_{0.75}Sr_{0.25}Fe_{12}O_{19}$ (BSFO) [6]. The substrate is produced by ceramic processing: the raw materials $BaCO_3$, $SrCO_3$, and Fe_2O_3 are ball milled in stoichiometric amount and the solid solution is produced via the Mixed Oxide synthesis method by calcination at different temperatures and soaking times, among those the optimal one resulted in heating at 900°C for 12 h. The powder is then attrition milled, sieved, and cold consolidated by die pressing at 400 kg/cm², followed by cold isostatic pressing at 3000 kg/cm². Heat treatment at 1250°C for 5 h results in sintered bodies with highest final relative density of about 96%. The SEM morphology of the sintered material is shown in Fig. 1.

Disks of different diameter and thickness were prepared for both permittivity and permeability measurements and for the prototype antenna (Fig. 2). The sintered samples (Fig. 2(a)) were grounded and punched (Fig. 2(b)). Metallizations were put on the top and bottom surfaces of the sample and connected by screen printing a silver paste, followed by heating at 750°C (Figs 2(c) and 2(d)).

B) Permittivity and permeability measurements

From the measured material characteristics, no effective FMR is visible up to 1 GHz; hence for the antenna design we exploited the measured behavior of permittivity and permeability in the frequency range 1 MHz–1 GHz to build the material model inside the EM simulation tool [8]. Indeed, we implemented our own material model by using a customized piecewise polynomial approximation, since no
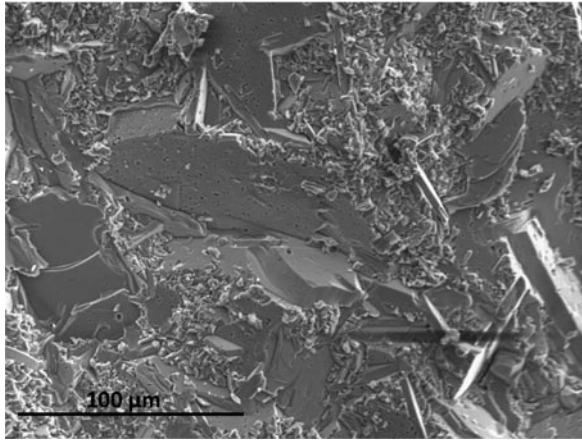
Fig. 1. SEM morphology of the sintered BSFO material.
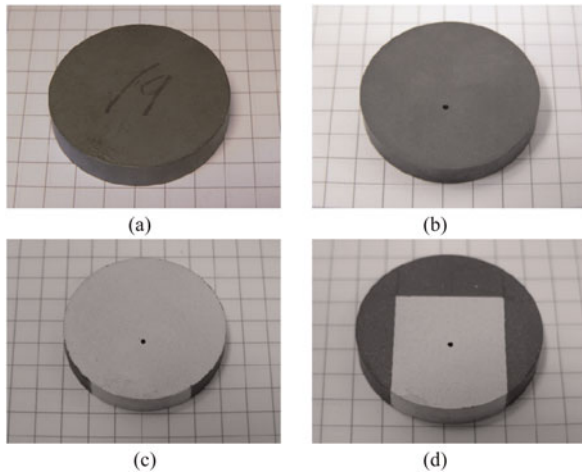
Fig. 2. BSFO sample (a) after sintering; (b) after grinding and punching; (c, d) after deposition of silver metallizations on both sides (via-hole is clearly visible).

satisfactory pre-defined model was available. The accuracy of this choice is clearly shown in Fig. 3: we were forced to make use of a relatively small band, 750–1000 MHz, to guarantee the best matching between the EM tool Lorentz dispersive model, and the measured values for ε', ε'', μ', and μ''. Considerable magnetic losses are observed which we expect to improve in a second material fabrication by means of optimization of the grain synthesis process. On the contrary, the dielectric losses show an acceptable behavior all over the measured band. At the design frequency of 868 MHz, the BSFO sample exhibits a value of $\varepsilon' \approx 12$ and a value of $\mu' \approx 2$, with dielectric loss tangent $\varepsilon''/\varepsilon' \approx 0.01$ and magnetic loss tangent $\mu''/\mu' \approx 0.38$. This results in a refraction index of 5 approximately; hence the reduced effective wavelength is $\lambda_g \approx \lambda_o/5$ (where λ_o is the free-space wavelength).

C) BSFO magnetization properties and FMR prediction

Once the whole characterization at high frequency was performed, the BSFO sample was broken into small pieces, one of which (of weight $w \approx 32.12$ mg) was used to measure the magnetic hysteresis loop $m(H)$, shown in Fig. 4, where m is the magnetic moment (in emu) and H is the magnitude of the applied magnetic field (in Oe). Since m is an extensive property mainly depending on the mass of the sample, in order to compare different samples it is necessary to use magnetization M, either mass magnetization M_m (measured in emu/g) or volume magnetization M_V (measured in emu/cm³) by calculating m/w or m/V, respectively. For the BSFO under test, the magnetic hysteresis loop, measured at room temperature, reveals a typical hysteresis for materials with random anisotropies. We registered a coercive field H_c of about 2577 Oe, (mass) saturation magnetization $M_{m,S}$ of about 60 emu/g (saturation is reached for $m \approx 1.84$ emu), (mass) remanent magnetization $M_{m,R}$ of about 34.11 emu/g and a squareness ratio SR ($SR = M_{m,R}/M_{m,S}$) of about 0.57. The latter values are in agreement with the ones
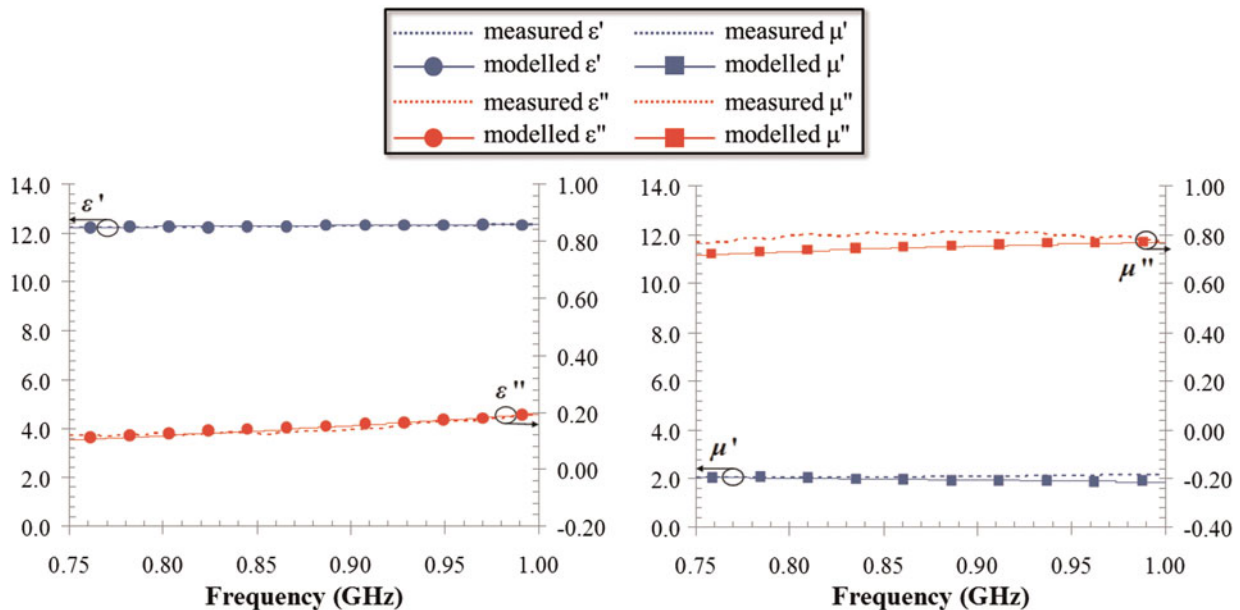
Fig. 3. Comparison between measured and modeled values of relative permittivity (left) and permeability (right) in the band 750 MHz–1 GHz.
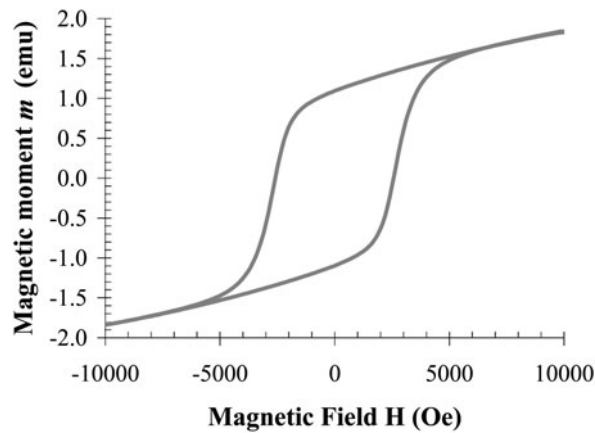
Fig. 4. Magnetic hysteresis loop for BSFO at room temperature (1 emu = 10^{-3} A·m², 1 Oe = $10^3/4\pi$ A/m).

experimentally determined for other BSFO materials [6]. Owing to the large H_c, hexaferrites are categorized as "hard" permanent magnets, since the non-zero value of m for $H =$ 0 Oe means a permanent magnetization of the material. Considering that the BSFO structure is equivalent to a magnetic system consisting of magnetic entities with randomly distributed magneto-crystalline anisotropy, from the value of H_c an approximate value of the anisotropy field H_K of about 5053 Oe is obtained, since

$$H_c \approx 0.51 H_K \text{ and } H_K = \frac{2K}{M_{m,S}}, \quad (5)$$

where K is the magneto-crystalline anisotropy constant.

To characterize the material w.r.t. its FMR and thus to establish the maximum feasible operating frequency, we experimentally investigated the magnetic losses at 10 GHz, therefore well above the selected frequency band of interest (the 10-GHz reference frequency was selected as the highest possible one compatible with the available instrumentation). A cavity with and without the BSFO sample was placed between two magnets and the magnetic field intensity was varied up to 9037.6 Oe, corresponding to a maximum value for magnetic induction B of 1 T. In the absence of the sample, no shift of the cavity resonance frequency was observed. When the cavity was filled with the sample, a resonance frequency shift and an attenuation of the specific reflection coefficient intensity $|S_{11}|$ were observed, demonstrating that magnetic losses are non-negligible but not high enough to significantly degrade $|S_{11}|$. These results allowed us to conclude that at 10 GHz the material losses are far from varying strongly and rapidly, which is the typical behavior around the FMR. The missing of the FMR peak at 10 GHz is expected for the BSFO, because for materials with a high value of H_K the resonance frequency $f_{res,Hk}$, which corresponds to the gyromagnetic lower limit of the absorption band [9], is expressed by equation (6):

$$f_{res,Hk} = \frac{\gamma}{2\pi} H_K \Rightarrow f_{res,Hk} \approx 14.15 \text{ GHz}, \quad (6)$$

and, consequently, the maximum magnetic energy absorption will be at a frequency higher than 10 GHz.

The magnetic permeability measurements were performed for samples in saturated/demagnetized state. It has to be stressed that the radiation properties of the antenna are related very closely to the magnetic permeability, which is a tensor for magnetic materials. Modifying the magnetization direction and amplitude, i.e. the magnetization state of the MD substrate, the overall radiation performance is changed accordingly.

III. ANTENNA DESIGN BY FULL-WAVE NUMERICAL SIMULATIONS AND PROTOTYPE REALIZATION

As reported in [10, 11], antennas with equivalent surface magnetic currents J_{ms} (such as patch antennas) are more suitable to be exploited with MD substrates, since the electric field E is the principal responsible for the radiation. Application of the Lowe's field equivalence principle allows us to replace the volume source of the transmitting antenna mainly with the equivalent magnetic surface currents only (which are not affected by μ_r):

$$J_{ms} = E \times \hat{n}. \quad (7)$$

This allows us to reach antenna miniaturization, allowing at the same time an overall size as stated in equation (1) with no significant reduction of radiation performance. Hence, under the assumption of negligible magnetic losses, the two main advantages of our choice are: (1) preserving radiation efficiency; (2) increasing in bandwidth (due to a lower quality factor Q). According to [12, 13], an 868 MHz patch antenna has been designed to test the engineered substrate, as this is a much exploited frequency for RFID applications in the UHF band in Europe. The BSFO sample used for our prototype is a disk, since round in shape devices are suitable for wearable applications thanks to the absence of sharp edges. To further enhance antenna miniaturization, a shorting-plate solution has been adopted, thus providing a $\lambda_g/4$-patch antenna: given $\lambda_o \approx 345.62$ mm at 868 MHz, we have $\lambda_g/4 \approx 18$ mm. The diameter for the disk was chosen equal to 33 mm, thus providing a substrate large enough for the patch antenna aperture. Finally, we have tackled two drawbacks: (1) the fragility of the ceramic composite when drilling a hole in the sample for antenna feeding; (2) the high dielectric permittivity of the material, which could degrade the radiating properties of the antenna. Thus, a substrate thickness of 5 mm has been chosen as the best trade-off between robustness against mechanical stress and EM behavior of the antenna. The curved shorting-plate was mounted on top of the substrate: this has turned out to be an easy-to-make solution that preserves antenna radiating properties, since the radiating aperture faces a bigger portion of substrate w.r.t. a centered patch. The patch, the shorting-plate, and the ground plane are made of a 4 µm-thick silver film. Antenna feeding is realized by inserting a micro-coaxial cable U.FL-LP-088 (50 Ω) into a via. An image exported from the EM simulator reporting the parameters used for the design is shown in Fig. 5, together with the final prototype of the antenna: the metallization dimensions of the patch are $L = 19.15$ mm (length) and $W = 17.65$ mm (width), the distance d between the via and the lower edge of the patch is 9.57 mm and the feeding-point radius is 440 µm. The overall weight of the designed prototype is about 20 g.
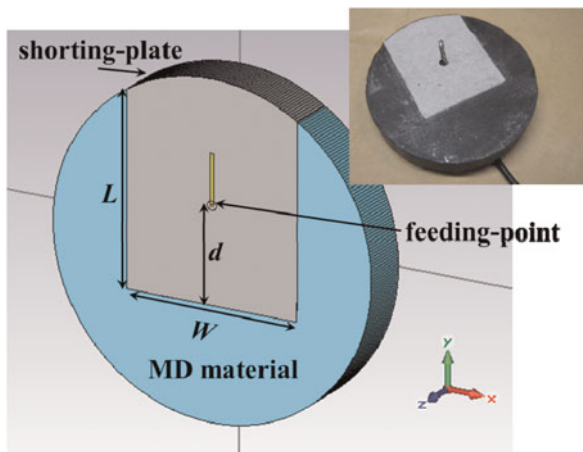
Fig. 5. Button-shaped patch antenna: EM model and view of the prototype.

The broadside radiation performance is preserved by extending the ground plane area of the BSFO-based patch. For this purpose, a 254 µm-thick EMC shielding conductive fabric, with conductivity $\sigma = 1 \times 10^7$ S/m, is attached to the patch ground plane [14]. This turns out to be an excellent choice to be exploited for any wearable application.

IV. EXPERIMENTAL CHARACTERIZATION: COMPARISON BETWEEN SIMULATIONS AND MEASUREMENTS

The effectiveness of our design and of the BSFO parameters characterization is discussed in this section with an extensive comparison with measured data. In Fig. 6, the surface currents plot is considered at the resonance frequency of 868 MHz. It clearly demonstrates that the designed antenna acts as a quarter-wavelength patch: the current nulls occur in correspondence to the lower radiating slot, and the current maxima are at the shorting-plate section. This also provides proof of the accuracy of material characterization.

In Fig. 7, a very good agreement between simulated and measured values of the reflection coefficient is demonstrated. In the band 750 MHz–1 GHz the two curves exhibit an $|S_{11}|$ lower than −10 dB all over the band: this corresponds to a relative bandwidth of 29%, which is the result of the designed substrate properties, whereas a typical characteristic of patch antennas is being narrow-band (about 4% of relative bandwidth in most cases). This could be considered as a great advantage in terms of both robustness of the antenna against mechanical tolerances and different standard applications. In Fig. 8, the E-plane (yz) and the H-plane (xz) simulated (blue solid line) and measured (red dotted line) normalized radiation patterns of the E-field at 868 MHz are plotted in polar coordinates, respectively, with the antenna mounted on the conductive fabric. A very good correspondence is observed in both two planes. The computed maximum directivity is about 6.4 dBi with a half-power beam width on the xz-plane of about 82°, whereas the radiation efficiency is 1.5%. The latter low value is mainly due to the magnetic losses and the electrically small characteristics required by our application purposes. However, the
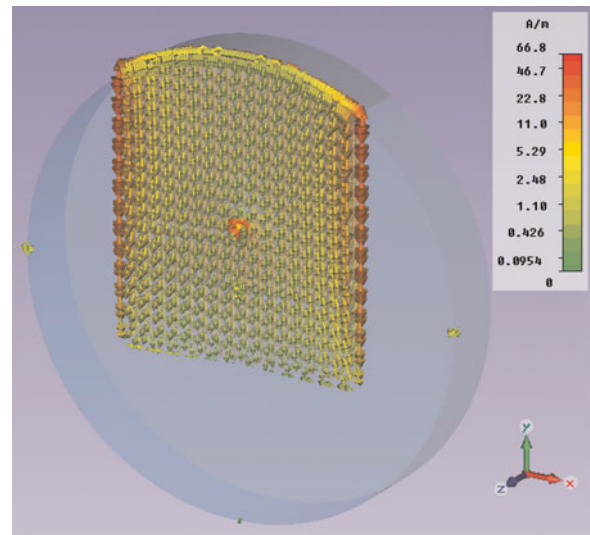
Fig. 6. Surface currents plot of the wearable patch antenna at resonance frequency of 868 MHz.

bandwidth-gain product is enhanced w.r.t. electrically small antennas on pure high-ε_r dielectric substrates. In turn, the overall antenna size is compatible with a jacket button (see Fig. 5). Furthermore, matching and radiating properties of the whole system, i.e. antenna and wearable substrate, are independent of the presence of human body which the system itself is attached to. This is the consequence of using the conductive shielding fabric which enhances antenna radiation performance and ensures EM compatibility at the same time. This is apparent in Fig. 8, where a very low front-to-back ratio is observed (the minimum measured value is −16.34 dB), thus ensuring negligible interactions between antenna and human body. Anyway, the antenna alone, directly placed on the human body without the conductive fabric, still guarantees a fairly good behavior. This is shown in Fig. 8 where the E-plane (yz) and the H-plane (xz) (green circles line) radiation patterns at 868 MHz computed in this situation are superimposed on those obtained for the antenna-on-conductive-fabric system. The maximum directivity is about 4.8 dBi, with a half-power beam width on the xz-plane of about 117° and a front-to-back ratio of about −8.5 dB. This entails two main results: (a) the idea of
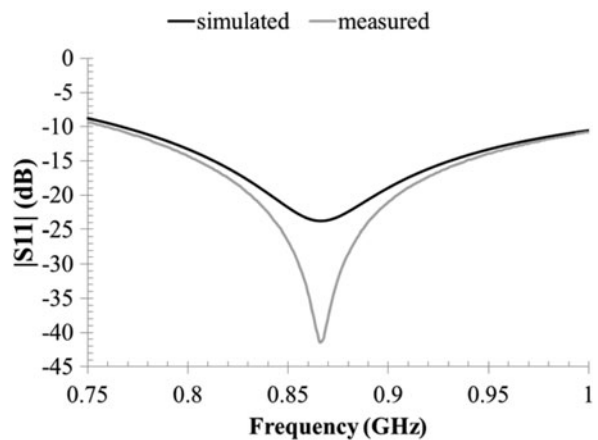
Fig. 7. Simulated and measured reflection coefficient in the band 750 MHz–1 GHz for the proposed MD antenna.
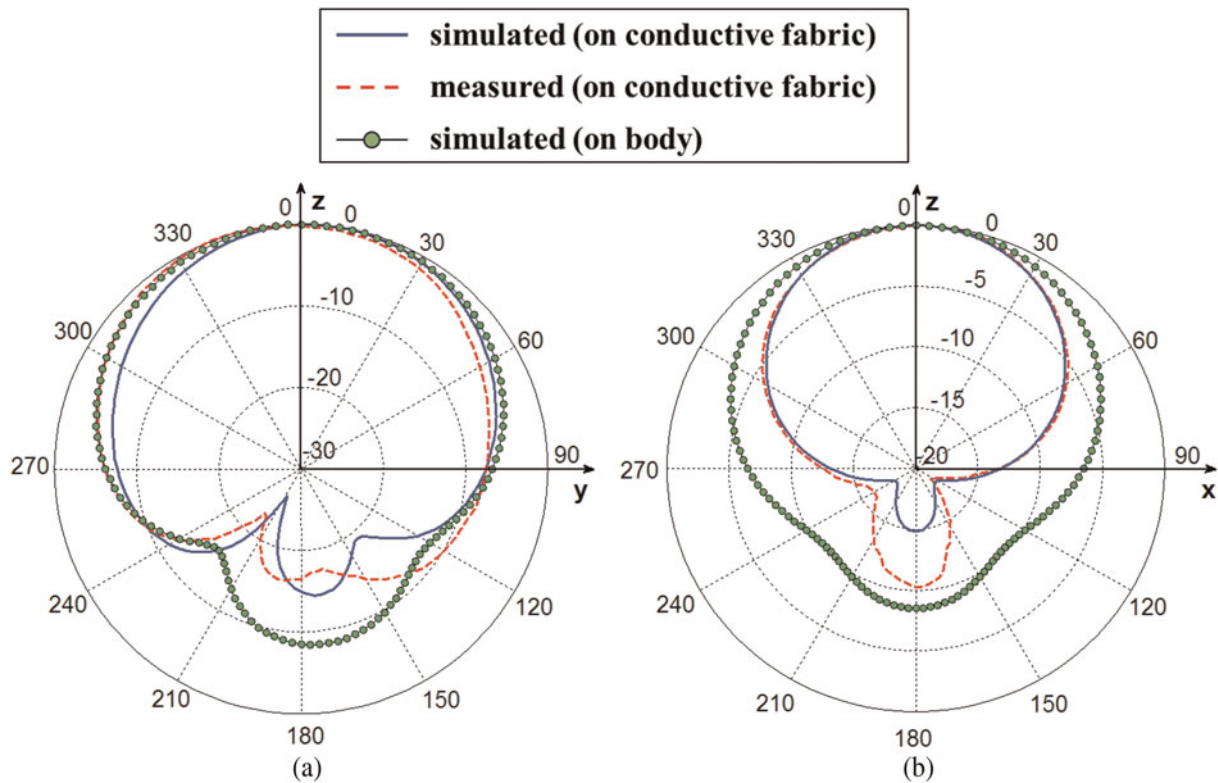
Fig. 8. (a) E-plane and (b) H-plane simulated and measured normalized radiation patterns of the proposed MD-based button antenna at 868 MHz, on a conductive fabric and placed directly on the body skin.
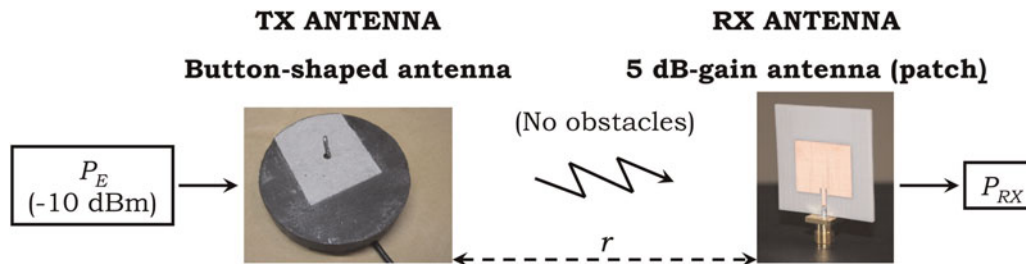
Fig. 9. Schematic view of the experimental set-up for link-budget measurements. r is the distance between antennas.

adopting a conductive fabric allows an easy-to-embed solution, but the skin itself acts as an extended ground plane which preserves the broadside radiation behavior of the antenna; (b) the (computed) directivity is only 1.5 dBi lower and the back-radiation still exhibits a negligible value for potential interactions with human tissues.

The radiation patterns in Fig. 8 have been measured at a 3-meters distance from the antenna: good correspondence between measurements and far-field simulations performance confirms that the far-field approximation is valid for the experimental set-up.

In order to validate the authors' conclusions that magnetic losses play a predominant role in antenna efficiency, we investigated the effect of silver thickness. The penetration depth of silver at resonance frequency is about 2.152 μm. Hence, metal thickness of the antenna is about two times the penetration depth, which is the minimum acceptable limit to avoid thin-conductor loss effects. For this purpose, we carried out simulations with increasing values of the silver thickness up to

35 μm: no significant improvement of radiation efficiency can be observed, thus giving an indirect proof of magnetic losses prevalence.

Finally, we investigated the feasibility of the proposed solution for wearable applications in indoor spaces. For this purpose, firstly we measured the power received by a 5 dB-gain antenna located at 1 m-distance ($r = 1$ m) from our MD button-type patch, with an emitted power P_E of -10 dBm (this is the input power at the antenna terminals): the experimental set-up is schematically shown in Fig. 9.

Table 1. Link-budget measurements for the experimental set-up displayed in Fig. 9.

Distance from RX antenna	Emitted power P_E (dBm)	Friis-calculated P_{RX} (dBm)	Measured P_{RX} (dBm)
1 m	-10	-46.1	-44
3 m	-10	-55.7	-55.6
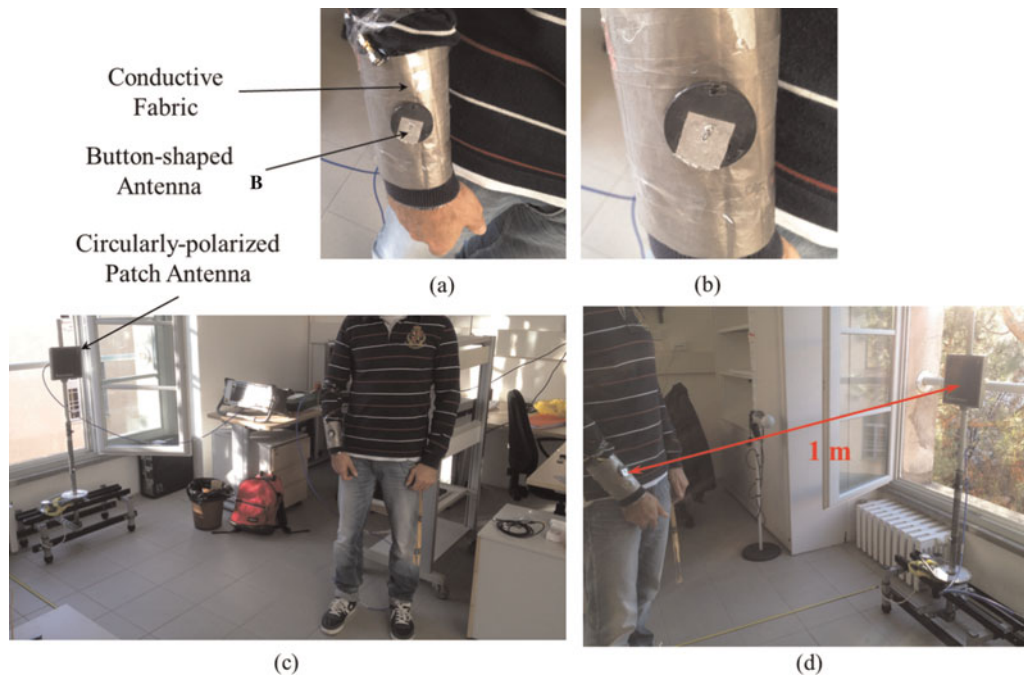
Fig. 10. Measurement set-up for the on-body (worn) solution: (a) overall radiating system worn on right arm; (b) detail of button-shaped antenna attached to conductive fabric; (c) measurement environment; (d) measurement example at 1 m-distance.

The space was kept free of obstacles and the receiving antenna was placed in the focus of a parabolic reflector in order to deal with reduced fading- and multipath effects. A received power P_{RX} of -44 dBm was measured, in good agreement with the results of the corresponding Friis calculations (-46.1 dBm); at a 3 m-distance ($r = 3$ m) the same quantity decreased to about -55.6 dBm (Table 1 summarizes the latter results). These received power levels allowed us to suppose that the proposed solution is well suitable for being exploited in indoor scenarios with links extension of a few meters, typical requirement of civil or healthcare spaces. For example, assuming a receiver sensitivity of -85 dBm, a 30 dB margin is preserved for potential scattering attenuation.

Secondly, in order to validate the link performance in a realistic rich-scattering indoor environment, we carried out power measurements with the on-body (worn) configuration (shown in Fig. 10) and with the off-body (not worn) one. In the two set-ups, the overall radiating system (button-shaped antenna and conductive fabric) is excited with $P_E = -10$ dBm and kept at various distances from a 6 dB-gain circularly-polarized patch antenna, connected to a Spectrum Analyzer in order to measure P_{RX}. The environment surrounding the measurement set-up (see Fig. 10) is characterized by many different obstacles which can be seen as "scatterers", thus representing a realistic operating mode of the device under test (DUT). We expect that the radiating performance of the button-shaped antenna does not change

significantly in the two situations (on-body and off-body) thanks to the conductive fabric attached to the patch ground plane. The experimental results are summarized in Table 2: a good agreement between the two set-ups can be observed, thus providing a proof of device reliability in terms of radiating performance and EM compatibility.

V. CONCLUSION

This contribution has introduced the synthesis of an innovative MD material (barium-strontium hexaferrite, BSFO) and its EM characterization to be adopted as the substrate for design of an electrically small, wearable patch antenna, in the 868-MHz band. First, we concentrated on material synthesis directed toward increase of the FMR with respect to previous exploited solutions. To reach this goal, hexaferrites components have been selected allowing higher FMR frequency due to their moderate values of relative permittivity and permeability, large anisotropy field, and low eddy-current losses. A first prototype has been fabricated and its near-field and far-field performance have been extensively investigated numerically and experimentally. Simulations and measurements of the prototype have shown a very good agreement. This result can be considered as the starting point for future research into the field of MD antennas, with innovative layouts, exploiting the magnetic properties of the substrates in the best way. In particular, the BSFO synthesis process is under development to improve substrate characteristics from the point of view of magnetic losses that significantly affect radiation efficiency behavior.

Table 2. Link-budget measurements for on- and off-body solution in a realistic propagation scenario.

Distance from RX antenna	Emitted power P_E (dBm)	On-body solution P_{RX} (dBm)	Off-body solution P_{RX} (dBm)
1 m	-10	-51.1	-53.4
2 m	-10	-57	-57.1
3 m	-10	-62.4	-64.3

REFERENCES

[1] Waterhouse, R.B.; Targonski, S.D.; Kokotoff, D.M.: Design and performance of small printed antennas. IEEE Trans. Antennas Propag., **46** (11) (1998), 1629–1633.

[2] Mosallaei, H.; Sarabandi, K.: Engineered meta-substrates for antenna miniaturization, in *URSI International Symposium on Electromagnetic Theory*, Pisa (Italy), May 2004.

[3] Mosallaei, H.; Sarabandi, K.: Design and modeling of patch antenna printed on magneto-dielectric embedded-circuit metasubstrate. IEEE Trans. Antennas Propag., **55** (1) (2007), 45–52.

[4] Ozgur, U.; Alivov, Y.; Morkoc, H.: Microwave ferrites, part 1: fundamental properties. J Mater Sci: Mater Electron, **20** (9) (2009), 789–834.

[5] Aldrigo, M.; Costanzo, A.; Masotti, D.; Galassi, C.: Exploitation of a novel magneto-dielectric substrate for miniaturization of wearable UHF antennas. Mater. Lett., **87** (2012), 127–130.

[6] Pereira, F.M.M. et al.: Magnetic and dielectric properties of the M-type barium-strontium hexaferrite ($Ba_xSr_{1-x}Fe_{12}O_{19}$) in the RF microwave (MW) frequency range. J Mater. Sci., Mater. Electron., **20** (2009), 408–417.

[7] Rizzoli, V.: Resonance measurement of single- and coupled microstrip propagation constants. IEEE Trans. Microw. Theory Tech., **25** (2) (1977), 113–120.

[8] CST Microwave Studio 2011, www.cst.com.

[9] Dionne, G.F.: Magnetic relaxation and anisotropy effects on high-frequency permeability. IEEE Trans. Magn., **39** (5) (2003), 3121–3126.

[10] Karilainen, A.O.; Ikonen, P.M.T.; Simovski, C.R.; Tretyakov, S.A.: Choosing dielectric or magnetic material to optimize the bandwidth of miniaturized resonant antennas. IEEE Trans. Antennas Propag., **59** (11) (2011), 3991–3998.

[11] Pacini, A.: Studio di topologie d'antenne su substrati magneto-dielettrici, B.Sc. thesis, Faculty of Engineering of Bologna, Cesena Campus, October 2012.

[12] Hansen, R.C.; Burke, M.: Antennas with magneto-dielectrics. Microw. Opt. Technol. Lett., **26** (2) (2000), 75–78.

[13] Aldrigo, M.; Bianchini, D.; Costanzo, A.; Masotti, D.; Galassi, C.; Mitoseriu, L.: New broadband button-shaped antenna on innovative magneto-dielectric material for wearable applications, in Proc. EuMW 2012, Amsterdam (NL), 28 October–2 November 2012.

[14] Costanzo, A.; Donzelli, F.; Masotti, D.; Rizzoli, V.: Rigorous design of RF multi-resonator power harvesters, in Proc. European Conf. Antennas and Propagation EUCAP 2010, Barcelona (Spain), April 2010.

[15] Ciomaga, C.E. et al.: Magnetoelectric ceramic composites with double-resonant permittivity and permeability in GHz range: a route towards isotropic materials. Scr. Mater., **62** (8) (2010), 610–612.

APPENDIX. MEASUREMENT SET-UP FOR BSFO CHARACTERIZATION

Two different set-ups were used for the permittivity and the permeability measurements. In this section, we refer to the sample as Device Under Test (DUT).

For the permittivity characterization, a disk of the BSFO material was deployed, with a diameter of 12.7 mm and thickness of 1.3 mm. The measurement procedure was based on two instruments: a Solartron 1296 Dielectric Interface in the band 1 Hz–1 MHz (Fig. 11(a)) and an Agilent E4991A RF Impedance/Material Analyzer in the band 1 MHz–1 GHz (Figs 11(b) and 11(c)) [15], to double validate measurements at 1 MHz.

At low frequencies, the dielectric measurements were carried out by recording the complex impedance of a fixture with parallel metallic plates filled with the DUT: in
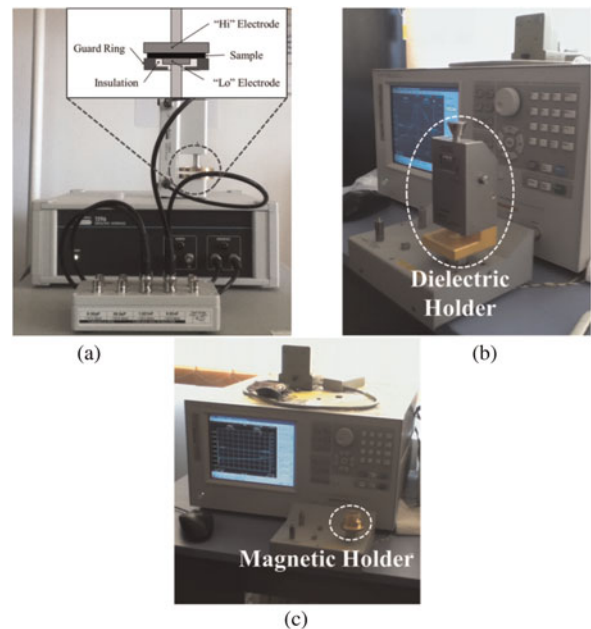
Fig. 11. (a) Low-frequency complex permittivity measurement set-up by the Solartron 1296 Dielectric Interface; high-frequency measurement set-up by the Agilent E4991A RF Impedance/Material Analyzer for (b) complex permittivity with dielectric holder Agilent 16453 and for (c) complex permeability with magnetic holder Agilent 16454A.

Fig. 11(a), the "Hi" electrode position is adjustable by means of a micrometer, whereas the "Lo" electrode position is fixed. The holder is equipped with a guard ring to ensure electric field homogeneity and prevent fringing effects at the edge of the DUT. In these conditions the structure is modeled as a capacitor and the complex permittivity is computed taking account of structure geometrical parameters.

At high frequencies, the impedance/material analyzer with dielectric holder Agilent 16453A shown in Fig. 11(b) was used, with the overall structure still configured as a parallel-plate capacitor. The dispersive G_p–C_p parallel circuit (where $G_p(\omega)$ is the equivalent parallel conductance representing dielectric losses, and $C_p(\omega)$ is the equivalent parallel capacitance) is used to derive complex permittivity from the measurements over a pre-established frequency band:

$$Y_c = G_p + j\omega C_p = j\omega\left(\frac{C_p}{C_o} - j\frac{G_p}{\omega C_o}\right)C_o, \quad (A1)$$

where Y_c is the measured complex admittance of the equivalent circuit and C_o is the capacitance when using air as DUT, then we have:

$$\varepsilon' = \frac{C_p}{C_o}, \quad (A2)$$

$$\varepsilon'' = \frac{G_p}{\omega C_o}. \quad (A3)$$

For the permeability characterization, a toroid-shaped DUT of the same BSFO material, 1.3 mm-thick with inner d_{DUT} and outer D_{DUT} diameter of 3.3 and 12.4 mm (respectively), was adopted. The permeability measurements were carried out by the same network analyzer: a conductive shield surrounding the central conductor and terminating in a short-circuit test

fixture TF (Agilent 16454A, referred to as "Magnetic Holder" in Fig. 11(c)) holds the toroid-shaped magnetic DUT. The central conductor is rolled once around the DUT and relative permeability is calculated from the inductance values at the end of the DUT itself. The magnetic field generated by the current flowing through the central wire is perpendicular to any cross section of the toroidal DUT. The short-circuit configuration ensures a maximum magnetic field and a minimum electric field near the DUT. The magnetic permeability is derived from the input impedance of the holder with and without the DUT. The complex impedance Z_c of a simple R_s–L_s series circuit can be used to model the measurement set-up: R_s is the equivalent series resistance that represents magnetic losses, and L_s is the equivalent series self-inductance of the measurement circuit. We also define: (1) the self-inductance L_{so} when a DUT is not mounted in the TF; (2) the thickness h of the DUT; (3) the radius r of the central wire; (4) the radius r_o of the TF; (5) the height h_o of the TF, then we have:

$$Z_c = R_s + j\omega L_s = j\omega\left(\frac{R_s}{j\omega} + L_s\right), \tag{A4}$$

$$\mu_r = \frac{2\pi(Z_c - j\omega L_{so})}{j\omega\mu_o\, h \ln\left(\frac{D_{DUT}}{d_{DUT}}\right)} + 1 \quad \Rightarrow \quad \mu' = \mathrm{Re}\{\mu_r\}, \tag{A5}$$

$$\mu'' = \mathrm{Im}\{\mu_r\},$$

$$L_{so} = \frac{\mu_o}{2\pi} h_o \ln\left(\frac{r_o}{r}\right). \tag{A6}$$

The dielectric and magnetic measurements were performed using the Agilent E4991A-002 software that provides direct readout of material parameters such as permittivity and permeability up to 1 GHz.

Martino Aldrigo obtained his M.Sc. degree (summa cum laude) in Telecommunications Engineering from the University of Bologna, Italy, in 2009. Since January 2011, he has been involved in a Ph.D. program at the same university. His main research interests are the design and project of miniaturized antennas and RF systems for wearable and implantable low-power applications, by exploiting innovative materials and energy-harvesting techniques. He is a member of the IEEE.

Alessandra Costanzo is an Associate Professor of Electromagnetic Fields at the University of Bologna, Cesena Campus, Bologna. She has co-authored more than 110 scientific publications on international journals and conferences and several chapter books. She holds two international licenced patents on remotely structural monitoring and on wearable antennas. Dr Costanzo's research interests are in the field of CAD tools for the electromagnetic-nonlinear co-design of RFIDs and near-field and far-field energy-harvesting

systems. She is a member of the MTT-24 RFID and of technical program committees of several international symposiums. She serves in the review board of several international journals. She is a member of the IEEE.

Diego Masotti received the Ph.D. degree in Electric Engineering from the University of Bologna in 1997. In 1998, he joined the Department of Electronics as a research associate. His research interests are in the area of microwave integrated circuit CAD, including nonlinear/electromagnetic co-design of integrated circuits and systems, and the development of general-purpose software tools for the signal and noise simulation of large nonlinear microwave subsystems. Dr Masotti has been a member of the Paper Review Board of the IEEE Transaction on Microwave Theory and Techniques since 2004 and is also a member of the IEEE.

Carlo Baldisserri received his M.Sc. degree in Physics from the University of Bologna in 2001 and his Ph.D. in 2007 from the Physics Department of the University of Limerick (Ireland). He has carried out work in the field of dielectric, pyroelectric, and piezoelectric characterization of several ceramic materials, deposition processes, and optical characterization of electrochemical interfaces, co-authoring four research papers in ICR refereed journals. He has been a post-doctoral Research Fellow at the National Research Council of Italy since 2009.

Ioan Dumitru received his Ph.D. in 2003 from the Physics department of University "Al. Ioan Cuza", Iaşi, Romania. Between 2003 and 2005 he was a Senior Researcher with the Advanced Material Research Institute, New Orleans, USA. Since 2007 he has been with the Faculty of Physics, University "Al. Ioan Cuza", Iaşi, Romania, where he is currently an Assistant Professor. His research interests mainly include high frequency measurement techniques for materials characterization, modeling in magnetism, magnetic materials, and microwave devices.

Carmen Galassi received her Diploma in Industrial Chemistry from the University of Bologna in 1981 and has been working at the National Research Council of Italy since 1984, and now is Senior Researcher. She is the coordinator of the project on ceramic materials for antenna miniaturization. 110 out of more than 200 of her authored papers are published in ICR refereed journals.